Strength, Fracture and Complexity 11 (2018) 137–148
DOI 10.3233/SFC-180219
IOS Press

The fracture of thermosetting epoxy polymers containing silica nanoparticles

F.J. Guild[a], A.J. Kinloch[a,*], K. Masania[a,†], S. Sprenger[b] and A.C. Taylor[a]
[a]*Department of Mechanical Engineering, Imperial College London, South Kensington Campus, London SW7 2AZ, UK*
[b]*Evonik Nutrition & Care GmbH, Charlottenburger Strasse 9, 21502 Geesthacht, Germany*

Abstract. An epoxy resin, cured with an anhydride, has been modified by the addition of silica nanoparticles. The particles were introduced via a sol–gel technique which gave a very well dispersed phase of nanosilica particles, which were about 20 nm in diameter, in the thermosetting epoxy polymer matrix. The glass transition temperature of the epoxy polymer was unchanged by the addition of the nanoparticles, but both the modulus and toughness were increased. The fracture energy increased from 77 J/m^2 for the unmodified epoxy to 212 J/m^2 for the epoxy polymer containing 20 wt.% of nanosilica. The fracture surfaces were inspected using scanning electron and atomic force microscopy, and these microscopy studies showed that the silica nanoparticles (a) initiated localised plastic shear-yield deformation bands in the epoxy polymer matrix and (b) debonded and allowed subsequent plastic void-growth of the epoxy polymer matrix. A theoretical model for these toughening micromechanisms has been proposed to confirm that these micromechanisms were indeed responsible for the increased toughness that was observed due to the presence of the silica nanoparticles in the epoxy polymer.

Keywords: Epoxy, fracture, modelling, nanoparticles

1. Background

When polymerised, epoxy polymers are amorphous and highly-crosslinked (i.e. thermosetting) materials and are typically used as adhesives and fibre-composite materials in the aerospace, automotive and electronic industries. This amorphous and highly-crosslinked microstructure results in many useful properties for structural engineering applications, such as a high modulus and failure strength, low creep, and good performance at elevated temperatures. However, this microstructure of thermosetting polymers also leads to one highly undesirable property in that they are relatively brittle materials, with a poor resistance to crack initiation and growth. Nevertheless, it has been well established (e.g. [1–3]) for many years that the incorporation of a second micro-phase of dispersed rubbery particles into the epoxy polymer can greatly increase their toughness, without significantly impairing the other desirable engineering properties. Typically the rubber particles are about 1–5 μm in diameter with a volume fraction of about 5–20%. However, the presence of such rubbery particles does somewhat decrease the modulus of the modified epoxy polymer and also typically leads to a significant increase in the viscosity of the liquid epoxy resin prior to curing. These effects often inhibit, for example, the use of the rubber-modified epoxy polymers as matrices for fibre composites. More recently, there has emerged a new technology which holds great promise for increasing the mechanical performance of such thermosetting polymers.

*Corresponding author. E-mail: a.kinloch@imperial.ac.uk.
†Present address: Complex Materials Group, Department of Materials, ETH Zürich, 8093 Zürich, Switzerland.

Namely, via the formation of a nanophase structure in the polymer, where the nanophase consists of rigid nanoparticles of silica [4]. The silica nanoparticles have an average particle diameter of about 20 nm.

In the present paper we report the substantial increase in toughness that may be achieved when such silica nanoparticles are well dispersed in a hot-cured single-part epoxy polymer. It should be noted that increasing the toughness of a hot-cured single-part epoxy polymer represents a far greater challenge than increasing the toughness of a two-part epoxy formulation [4]. This is because the former invariably has a significantly higher glass transition temperature, T_g, and a lower molecular-weight between crosslinks; and both of these features inhibit toughening of the epoxy polymer [5]. Further, the micromechanisms that are responsible for the observed increases in toughness are identified and are quantitatively modelled.

2. Experimental studies

2.1. Materials

The materials were based upon a hot-cured single-part epoxy formulation. The epoxy resin was a standard diglycidyl ether of bis-phenol A (DGEBA) with an epoxy equivalent weight (EEW) of 185 g/mol, namely 'Epikote 828' supplied by Hexion Speciality Chemicals, Germany. The silica (SiO_2) nanoparticles were supplied as a colloidal silica-sol in the resin matrix, 'Nanopox F400', by Evonik Nutrition & Care GmbH, Germany. The silica nanoparticles are synthesised from an aqueous sodium silicate solution [6,7]. They then undergo a process of surface modification with organosilane and matrix exchange, to produce a masterbatch of 40 wt.% of silica nanoparticles in the epoxy resin. The silica nanoparticles had a mean particle diameter of about 20 nm, with a narrow range of particle-size distribution: laser light scattering showed that almost all particles are between 5 and 35 nm in diameter. The particle size and excellent dispersion of these silica particles remain unchanged during any further mixing and/or blending operations. Further, despite the relatively high silica concentration of 40 wt.%, the nanofilled epoxy resin still has a comparatively low viscosity due to the agglomerate-free colloidal dispersion of the nanoparticles in the resin. The curing agent was an accelerated methylhexahydrophthalic acid anhydride, namely 'Albidur HE 600' supplied by Evonik Nutrition & Care GmbH, Germany. Plates of the unmodified epoxy and nanoparticle-modified epoxy were produced to determine the properties of the polymers. Firstly, the simple DGEBA resin was mixed together with given amounts of the nanosilica-containing epoxy resin, in order to produce a range of epoxy polymers with varying concentrations of silica nanoparticles, see Table 1. The value of the EEW of the blend was then measured, via titration. Secondly, the stoichiometric amount of the curing agent was added to the mixture, which was poured into release-coated moulds and cured for 1 hour at 90°C, followed by a post-cure of 2 hours at 160°C. The densities of the plates produced were measured using an Archimedes approach. An epoxy density of 1100 kg/m^3 and a silica density of 1800 kg/m^3 were calculated. The volume fraction of silica was calculated from the known weight fractions using the measured densities.

2.2. Glass transition temperature

The glass transition temperatures, T_g, of the unmodified epoxy polymer and the silica-nanoparticle modified epoxy polymers were measured using dynamic mechanical thermal analysis (DMTA). This was undertaken employing a 'Q800' machine from TA Instruments, UK, using 48 × 3 × 2 mm specimens in a three-point bending mode at 1 Hz. The storage modulus, loss modulus and loss factor, tan δ, were

Table 1
Glass transition temperature, Young's modulus, fracture toughness and fracture energy of the unmodified epoxy polymer and the epoxy polymers containing silica nanoparticles

Silica content (wt.%)	T_g (°C)	E (GPa)	K_c (MPa · m$^{1/2}$)	G_c (J/m^2)
0	153	2.96	0.51	77
4	152	3.20	0.64	123
7.8	154	3.42	0.79	179
11	151	3.57	0.80	183
15	152	3.60	0.83	191
20	150	3.85	0.88	212

calculated as a function of temperature for the range 40–175 °C. The glass transition temperature, T_g, was determined as the maximum stationary point of the tan δ versus temperature curve.

2.3. Mechanical properties

Tensile dumbbell specimens were machined from the plates. These were tested at a displacement rate of 1 mm/min and a test temperature of 21°C, according to the ISO standard test method [8,9]. The strain in the gauge length was measured using a clip-on extensometer, and the Young's modulus, E, was calculated. Plane-strain compression tests, as described by Williams and Ford [10], were conducted (a) to examine the ability of the epoxy polymers to undergo plastic deformation and (b) to ascertain the yield stress and post-yield behaviour. Tests were conducted using 3 × 60 × 40 mm specimens loaded in compression between two parallel, 12 mm wide, platens and were conducted at a constant displacement rate of 0.1 mm/min, and the results were corrected for the compliance of the machine and test rig.

2.4. Fracture testing

The single-edge notch bend (SENB) test was used to determine the mode I fracture toughness, K_c, at the onset of crack growth of the polymers. Specimens were machined from the sheets, and the fracture toughness was determined according to the relevant ISO standard [11], using a displacement rate of 1 mm/min and a test temperature of 21°C. Four replicate specimens were tested for each blend composition. The machined notch was sharpened by tapping a razor-blade into the machined notch before testing. All the specimens failed by unstable crack growth, and hence only a single, initiation, value of the fracture toughness was obtained from each specimen. The coefficient of variation in the values of K_c was ±10%. The value of the fracture energy, G_c, was calculated from knowledge of the values of K_c and E using the relationship:

$$G_c = \frac{K_c^2}{E}(1 - \upsilon^2) \tag{1}$$

where E is the modulus of elasticity obtained from the tensile tests and υ is the Poisson's ratio of the polymer, taken to be 0.35 [12].

2.5. Microscopy studies

The fracture surfaces of the SENB specimens were investigated at a relatively low magnification using scanning electron microscopy (SEM). A JEOL 'JSM-5300' scanning microscope was used and all specimens were coated with a thin layer of sputtered gold before analysis to prevent charging. An acceleration voltage of 20 kV was used. High resolution SEM was undertaken of the fracture surfaces using an electron microscope equipped with a field emission gun (FEG-SEM). The instrument used was a 'Leo 1525' from Carl Zeiss equipped with a 'Gemini' column. Typically, the acceleration voltage was set at 5 kV. All specimens were coated with an approximately 5 nm thick layer of gold or platinum before analysis. Also, thin sections, approximately 60–80 nm thick, of the blends were cryo-microtomed (at −50°C) for subsequent examination using transmission electron microscopy (TEM). The TEM was performed using a JEOL 'JEM-2000FX II' electron microscope at an acceleration voltage of 200 kV. Atomic force microscopy (AFM) studies were undertaken using a 'MultiMode' scanning probe microscope from Veeco equipped with a 'J' scanner and a 'NanoScope IV' controller. A smooth surface was first prepared by cutting samples using a cryo-ultramicrotome at temperatures down to −100°C. The scans were performed in tapping mode using silicon probes, and both height and phase images were recorded.

3. Results

3.1. Microstructure

Microscopy of the polymers showed that the unmodified epoxy was a homogeneous thermoset polymer, see Fig. 1a. A glass transition temperature, T_g, of 153°C was measured using dynamic mechanical thermal analysis, see Table 1. For the epoxy polymers containing the silica nanoparticles, there was no significant agglomeration of the 20 nm diameter silica nanoparticles particles at any concentration of nanoparticles, as illustrated in Fig. 1b. The glass transition temperatures of the epoxy polymers modified with the silica nanoparticles were unchanged, within the experimental uncertainty of ±2°C, from the value of the unmodified epoxy polymer. Similar results, showing no change in T_g due to the addition of silica nanoparticles, have been reported by other authors [13,14]. It should be noted that an increase in the T_g due to the addition of nanoparticles would be expected if the interaction between the polymer and the nanoparticles was strong. However, Baller et al. [14] have shown that the interaction between similar silica nanoparticles and an epoxy polymer matrix is relatively weak.

3.2. Basic mechanical properties

The values of the Young's modulus, E, measured from the tensile tests are summarised in Table 1. A modulus of 2.96 GPa was measured for the unmodified (i.e. control) epoxy polymer. The addition of silica nanoparticles increased the modulus as expected, since the modulus of silica, E = 70 GPa, is much greater than that of the epoxy polymer. A maximum modulus of 3.85 GPa was measured for the polymer containing 20 wt.% of silica nanoparticles, which is an increase of about 30% compared to that of the unmodified epoxy polymer.

3.3. Toughness

A fracture energy, G_c, of 77 J/m^2 was measured for the unmodified epoxy polymer. The fracture energy was increased by the addition of silica nanoparticles, and a maximum G_c, of 212 J/m^2 was measured for

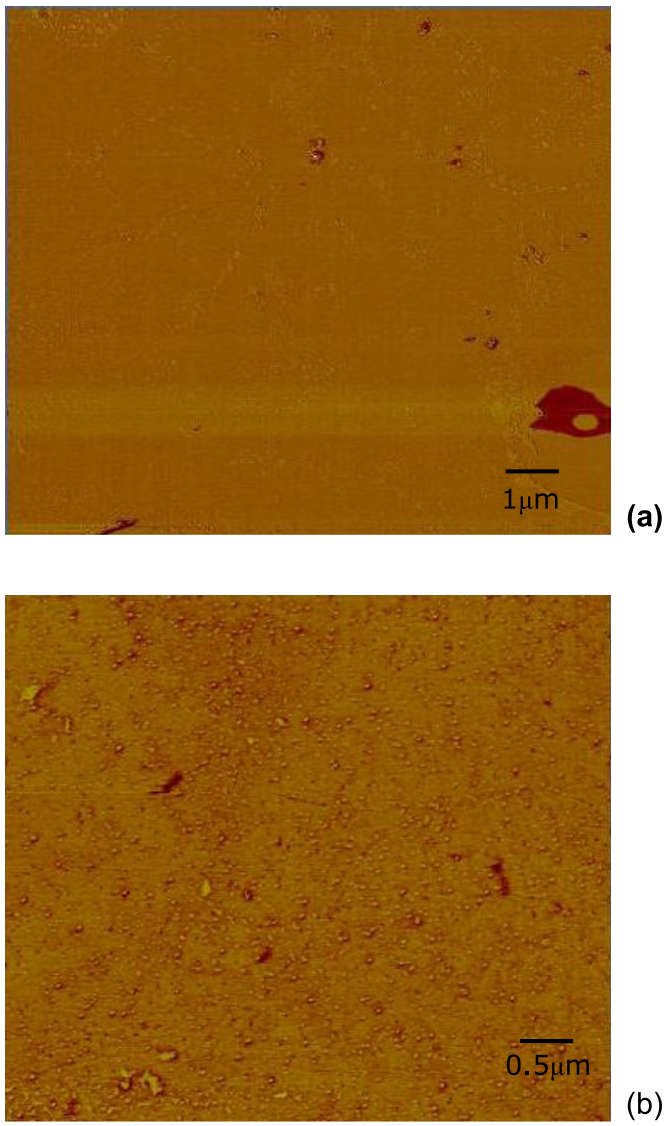

Fig. 1. AFM images of the microstructure of the epoxy polymers: (a) unmodified and (b) containing 11 wt.% silica nanoparticles.

the epoxy containing 20 wt.% of silica, as shown in Table 1. For completeness, the measured values of the fracture toughness, K_c, are also shown in Table 1, and these data show similar increasing trends with increasing silica nanoparticle concentration.

3.4. Plane-strain compression tests

An optical micrograph, taken between crossed polarisers, of a thin slice of the epoxy polymer containing 11 wt.% of silica nanoparticles is shown in Fig. 2. For clarity this is taken at the edge of the sample under plane-stress conditions, as the plastic zone under plane-strain conditions was too small to image satisfactorily. The corresponding conventional transmission optical-micrograph is shown in Fig. 2b, which

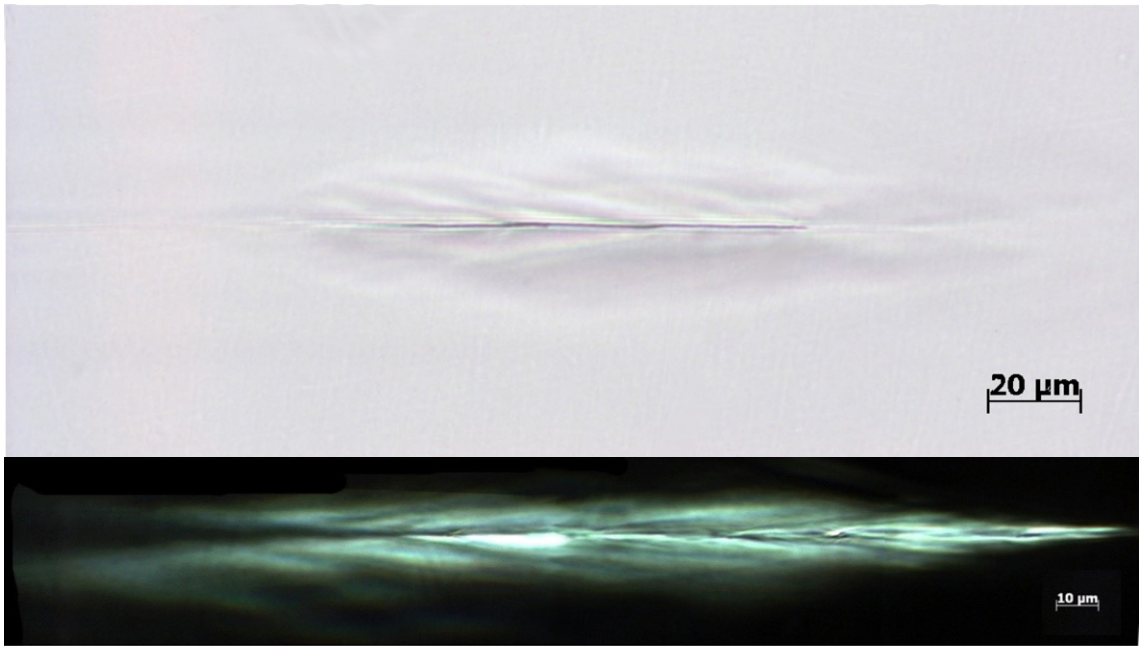

Fig. 2. Transmission optical-micrographs of an epoxy polymer containing 11 wt.% silica nanoparticles, showing the plane-stress region taken using (a) normal light, and (b) between crossed polarisers. (Crack propagation is from left to right.)

shows clearly the plastic deformation that has occurred in the epoxy polymer immediately ahead of the crack tip. This micrograph is very similar to those shown by previous authors [15] for dispersed rubber microparticles in an epoxy polymer, but these particles were of the size of micrometres, as opposed to the present silica nanoparticles which have a radius of 10 nm. The birefringence of the plastically-deformed polymer in the micrograph in Fig. 2b clearly reveals the plastic deformation that has occurred. The region closest to the fracture plane is relatively intense in nature, whilst the outermost regions suggest that the deformation occurs in micro-plastic shear-bands, which appear to merge to form diffuse regions.

The size of the plastic zone can be measured from these micrographs and compared to theoretical predictions. The Irwin model states that the radius of the plastic zone, r_y, can be calculated using [16]:

$$r_y = \frac{1}{k\pi}\frac{EG_C}{\sigma_y^2} \tag{2}$$

where E is the Young's modulus, G_c is the fracture energy, υ is the Poisson's ratio and σ_y is the tensile yield stress of the polymer. The constant, k, has a value of $k = 6(1 - \nu^2)$ for plane-strain conditions, and $k = 2$ for plane stress. For the epoxy polymer containing 11 wt.% of silica nanoparticles then we obtain a predicted value of r_y in plane strain of 4.8 µm, and a plane stress value of r_y = 14.4 µm. Experimentally, it was not possible to measure the plane-strain value as the plastic zone was too small, as noted above. However, the value of r_y measured in plane stress from the micrographs in Fig. 2 was 15 ± 2 µm. Thus, there is excellent agreement between the predicted and the experimental values. Similar very good agreement has been observed by Liang and Pearson in their work [13].

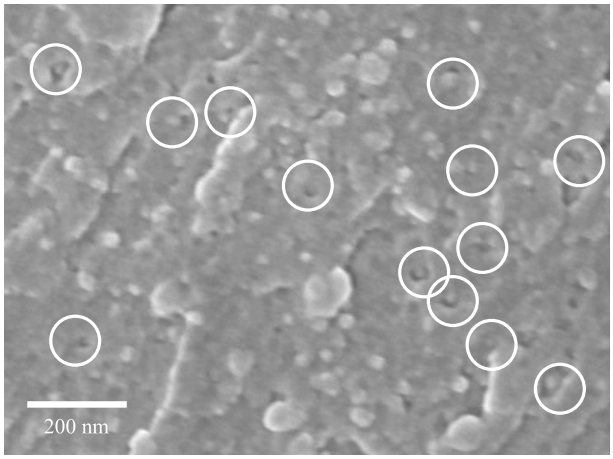

Fig. 3. High-resolution scanning electron micrograph of the fracture surface of the epoxy polymer containing 15 wt.% silica nanoparticles. (Some voids around the silica nanoparticles are circled.)

3.5. Fractographic studies

The fracture surface of the unmodified epoxy polymer was relatively smooth and glassy, which is typical of a brittle thermosetting polymer [17]. This shows that no large-scale plastic deformation has occurred during fracture, and reflects the relatively low value of the measured fracture energy, G_c. Feather markings were present, which were visible as steps and changes of the level of the crack. These are caused by crack forking due to the excess of energy associated with the rapid crack growth that occurred. This repeated forking, and the multi-planar nature of the surface, are ways of absorbing excess energy in a very brittle material [18].

Although the fracture energy was increased by the presence of silica nanoparticles, scanning electron microscopy of the fracture surfaces at a relatively low magnification showed no significant differences in the fracture surfaces when compared to the unmodified epoxy polymer. However, the silica nanoparticles cannot be seen at a low magnification due to their small diameter. Thus, high-resolution scanning electron microscopy (i.e. FEG-SEM) was employed. The resulting image of a fracture surface of the epoxy containing 15 wt.% of silica nanoparticles clearly showed the presence of voids around the silica nanoparticles, as is illustrated in Fig. 3. It should be noted that these voids are not an artefact of the coating process (which is used to prevent the sample charging during the electron microscopy investigations), since they were not observed on a coated fracture-surface of the unmodified epoxy [19]. The appearance of the voids was also independent of which coating material was used. Furthermore, the voids were also observed using AFM of the uncoated fracture-surfaces [19]. Now, it is noteworthy that not all of the silica nanoparticles appeared to debond to form voids. This observation may be explained from a finite element analysis model of the microstructure of the epoxy polymers containing the silica nanoparticles. Such modelling has demonstrated [20] that once one silica nanoparticle debonds then its nearest neighbours are shielded from the applied stress field, and hence may not debond. Statistical analysis showed that, for a good, i.e. random, dispersion of nanoparticles then each nanoparticle has six nearest neighbours, so only one in seven particles would be predicted to debond. This modelling approach therefore predicts that only 14.3% of the nanoparticles present will debond. This predicted value is in excellent agreement with the

measured value of 10–15% of those nanoparticles which are present and do debond, as was determined via direct observations of the fracture surfaces such as that shown in Fig. 2.

4. Toughening micromechanisms

From the above results, the toughening micromechanisms arise from the ability of the silica nanoparticles to induce an increased extent of plastic deformation of the epoxy polymer matrix. The two types of plastic deformation mechanisms in the epoxy polymer are: (a) localised plastic shear-bands initiated by the stress concentrations around the periphery of the silica nanoparticles and (b) debonding of the silica nanoparticles followed by subsequent plastic void-growth of the epoxy polymer matrix. These two deformation mechanisms, both of which involve the epoxy polymer undergoing localised plastic-deformation as a result of the silica nanoparticles being present in a 'process' or 'plastic' zone ahead of the crack tip, are quantitatively modelled below.

5. Theoretical studies

5.1. Introduction

The micromechanisms of plastic shear-band yielding and plastic void-growth arising from the presence of the silica nanoparticles in the epoxy polymer may be probed using a modelling approach successfully developed by Huang and Kinloch [21,22] for rubber-modified epoxy polymers. They proposed a generalised solution to examine incremental increases in G_c, where:

$$G_c = G_{cu} + \Psi \tag{3}$$

where G_{cu} is the fracture energy of the unmodified epoxy polymer and Ψ represents the overall contributions from the various toughening mechanism that are operative. The term Ψ was expanded to give:

$$\Psi = \Delta G_s + \Delta G_v \tag{4}$$

where the two terms on the right-hand side of Eq. (2) may be analytically derived and represent, respectively:
ΔG_s: the contribution from localised plastic shear-yielding in the epoxy polymer matrix initiated by the silica nanoparticles;
ΔG_v: the contribution from plastic void-growth in the epoxy polymer matrix associated with the silica nanoparticles debonding.

5.2. The contribution from the localised plastic shear-yielding micromechanism

The energy contribution, ΔG_S, from the localised plastic shear-banding initiated by the presence of the particles is related to the size of the plastic zone and was calculated by Huang and Kinloch [22] from the following equation:

$$\Delta G_s = 2 \int_o^{r_y} U_s(r) dr \tag{5}$$

where r_y is the radius the plastic zone ahead of the crack tip and $U_s(r)$ is the dissipated strain-energy density for the shear-yielding mechanism. However, it has been suggested that the lower limit of integration in Eq. (5) should not be zero. Instead, Evans et al. [23] proposed that the lower limit of integration should be the minimum distance from the crack plane at which the epoxy polymer between the particles experiences plastic shear-yielding. This distance was suggested to be of the order of the particle radius, since a crack typically passes around one pole of the particle, leaving the plastically-deformed polymer at the opposite pole. Thus, Eq. (5) now becomes:

$$\Delta G_s = 2 \int_{rp}^{r_y} U_s(r) dr \tag{6}$$

where r_p is the radius of the particle. According to the work of Dekkers and Heikens [24,25], shear bands will initiate from all of the particles. With the lower integration limits of r_p, instead of zero, the expression for the term ΔG_S is [26]:

$$\Delta G_s = 0.5 V_f \sigma_{yc} \gamma_f F'(r_y) \tag{7}$$

where V_f is the volume fraction of particles, σ_{yc} and γ_f are the plane-strain compressive yield stress and strain to fracture for the unmodified epoxy polymer, respectively. The term $F'(r_y)$ is given by [26,27]:

$$F'(r_y) = r_y[(4\pi/3V_f)^{1/3}(1 - r_p/r_y)^3 - (8/5)(1 - r_p/r_y)(r_p/r_y)^{5/2} - (16/35)(r_p/r_y)^{6/2} - 2(1 - r_p/r_y)^2 + (16/35)] \tag{8}$$

and where [22] :

$$r_y = K_{vm}^2 (1 + \mu_m/3^{1/2})^2 r_{yu} \tag{9}$$

where K_{vm} is the maximum stress concentration for the von Mises stresses around a rigid particle, μ_m is a material constant which allows for the pressure-dependency of the yield stress [28] and r_{yu} is the plastic zone size at fracture for the unmodified epoxy polymer. The value of K_{vm} is dependent on the volume fraction of particles, and was calculated by fitting to the data of Guild and Young [29]. Its value varies from approximately 1.60 to 1.73 over the range of volume fractions used in the present work. The value of r_{yu} may be readily calculated from [30]:

$$r_{yu} = \frac{1}{6\pi} \frac{EG_C}{(1 - \upsilon^2)\sigma_y^2} \tag{10}$$

where E, υ and σ_y are the modulus, Poisson's ratio and tensile yield stress of the unmodified epoxy polymer, respectively. All the parameters in Eqs (3)–(10) may be measured or directly calculated as shown in Table 2. Thus, the contribution ΔG_S may be readily ascertained.

5.3. The contribution from the plastic void-growth micromechanism

For nanoparticles, the debonding process is generally considered to absorb very little energy compared to the plastic deformation of the epoxy polymer matrix [12,31]. However, debonding is essential because this allows the epoxy polymer to deform plastically via a plastic void-growth mechanism. The energy contribution, ΔG_v, from the plastic void-growth mechanism is related to the size of the plastic zone and

Table 2
The parameters, and their values, used in the modelling studies

Name	Symbol	Unit	Value	Source
Radius of the silica nanoparticles	r_p	nm	10	[19]
Volume fraction of the nanoparticles	V_f	-	See Table 2	Present study
Volume fraction of the particles which debond and void	V_{fp}	-	0.15 V_f	Present study
Radius of voids around the debonded nanoparticles	r_{pv}	nm	15	[19]
Tensile modulus	E	GPa	2.96	Present study
Poisson's ratio	υ	–	0.35	[12]
Plane-strain compressive yield stress	σ_{yc}	MPa	138	Present study
Plane-strain compressive fracture strain (true strain)	γ_f	-	0.65	Present study
Uniaxial tensile yield stress	σ_y	MPa	88	Present study
Pressure-dependent yield stress parameter	μ_m	–	0.2	[28]
Fracture energy	G_c	J/m^2	77	Present study

Note: All mechanical properties are for the unmodified epoxy polymer.

was calculated by Huang and Kinloch [22] from the following equation:

$$\Delta G_\upsilon = 2\int_o^{r_y} U_\upsilon(r)dr \tag{11}$$

where r_y is the radius the plastic zone ahead of the crack tip and $U_v(r)$ is the dissipated strain-energy density for the plastic void-growth mechanism. The modelling studies of Huang and Kinloch [22] give the contribution ΔG_V to the toughness from the plastic void-growth mechanism as:

$$\Delta G_\upsilon = (1-\mu_m^2/3)(V_{f\upsilon} - V_{fp})\sigma_{yc} r_{yu} K_{\upsilon m}^2 \tag{12}$$

where V_{fv} and V_{fp} are the volume fraction of voids and the volume fraction of particles which debond, respectively. The term V_{fp} was taken to be 15% of the volume fraction, V_f, of the silica nanoparticles that were present, as calculated from the finite-element analysis modelling, as described above. It may be recalled that these calculations were in excellent agreement with the measured values from the FEG-SEM studies. To obtain the value of the volume fraction of voids, V_{fv}, it is noteworthy that the void size measured from the high-resolution electron micrographs can be compared to values calculated from considering the maximum hoop strain around the particles. If the fracture strain measured from the plane-strain compression tests, i.e. a true strain of 0.65, is equated with the maximum hoop strain around the void, then a final void diameter of 33 nm is predicted. This compares very well with the mean diameter of 30 nm which was measured from the micrographs. Thus, the value of V_{fv} may be readily calculated by direct measurement or by such a calculation.

5.4. Application of the model

The value of Ψ may now be evaluated from Eqs (5) and (12) to give, via Eq. (4):

$$\Psi = 0.5 V_f \sigma_{yc} \gamma_f F'(r_y) + (1-\mu_m^2/3)(V_{f\upsilon} - V_{fp})\sigma_{yc} r_{yu} K_{\upsilon m}^2 \tag{13}$$

where the all the parameters may be directly measured or calculated, as described above, and are given for the present epoxy polymers in Table 2. Hence, the value of the fracture energy, G_c, of the epoxy polymers may be predicted from Eqs (3) and (13). The predicted values are compared to the experimentally

Table 3
Comparison of the measured and predicted values of the fracture energy, G_c, as a function of the concentration of silica nanoparticles in the epoxy polymer

Silica content (wt.%)	Silica content (V_f)	ΔG_s (Eq. (7)) (J/m^2)	ΔG_v (Eq. (12)) (J/m^2)	G_c (Eqs (3) + (4) + (13)) (J/m^2)	G_c (measured) (J/m^2)
0	0	–	–	–	77
4.0	0.025	45	6	128	123
7.8	0.049	64	11	152	179
11	0.071	76	16	169	183
15	0.096	87	21	185	191
20	0.134	98	31	206	212

measured values in Table 3 and, as may be observed, there is very good agreement between the measured values and those predicted from the model proposed above. Indeed, this good agreement is especially noteworthy when the lack of any adjustable fitting terms in the above equations is considered.

6. Conclusions

The structure/property relationship of an anhydride-cured epoxy modified with silica nanoparticles has been investigated. Microscopy showed that the silica nanoparticles were well-dispersed in the epoxy. The fracture energy, G_c, of the bulk epoxy was increased from 77 to 212 J/m^2 by the addition of 20 wt.% silica nanoparticles. The observed toughening mechanisms were (a) localised plastic shear-bands in the epoxy polymer matrix initiated by the stress concentrations around the periphery of the silica nanoparticles, and (b) debonding of the silica nanoparticles followed by subsequent plastic void-growth of the epoxy polymer matrix. A model has been proposed to predict these toughening micromechanisms induced by the presence of the silica nanoparticles in the thermosetting epoxy polymer matrix. There was excellent agreement between the predictions and the experimental data for the epoxy polymers containing silica nanoparticles.

Acknowledgements

This paper was presented at the 'Special Symposium' held at 'ICF14, Rhodes, Greece' to mark the outstanding contributions of David Taplin to the International Congress of Fracture (ICF) over the past fifty years.

Conflict of interest

None to report.

References

[1] E.H. Rowe, A.R. Siebert and R.S. Drake, Toughening thermosets with butadiene/acrylonitrile polymers, *Modern Plastics* **47** (1970), 110–117.

[2] R.S. Drake and A.R. Siebert, Elastomer-modified epoxy adhesives for structural applications, *SAMPE Quart.* **6**(4) (1975), 11–21.

[3] A.J. Kinloch, S.J. Shaw, D.A. Tod and D.L. Hunston, Deformation and fracture behaviour of a rubber-toughened epoxy: 1. Microstructure and fracture studies, *Polymer* **24** (1983), 1341–1354.
[4] A.J. Kinloch, J.H. Lee, A.C. Taylor, S. Sprenger, C. Eger and D. Egan, Toughening structural adhesives via nano- and micro-phase inclusions, *J. Adhesion* **79** (2003), 867–873.
[5] A.J. Kinloch, Theme article - toughening epoxy adhesives to meet today's challenges, *Mater. Res. Soc. Bull.* **28** (2003), 445–448.
[6] HanseChemie, Patent Application, Patent Application WO 02/083776 A1, 2002.
[7] S. Sprenger, C. Eger, A.J. Kinloch, A.C. Taylor, J.H. Lee and D. Egan, Nanoadhesives: Toughness and high strength, *Adhaesion, Kleben & Dichten* **3** (2003), 24–28.
[8] ISO-527-1, Plastics - Determination of tensile properties - Part 1: General principles, International Standards Organisation: Geneva, 1993.
[9] ISO-527-2, Plastics - Determination of tensile properties - Part 2: Test conditions for moulding and extrusion plastics, International Standards Organisation: Geneva, 1996.
[10] J.G. Williams and H. Ford, Stress-strain relationships for some unreinforced plastics, *J. Mech. Eng. Sci.* **6** (1964), 405–417.
[11] ISO-13586, Plastics - Determination of fracture toughness ($G_{IC}K_{IC}$) - Linear elastic fracture mechanics (LEFM) approach, International Standards Organisation: Geneva, 2000.
[12] A.J. Kinloch, *Adhesion and Adhesives: Science and Technology*, Chapman & Hall, London, 1987.
[13] Y.L. Liang and R.A. Pearson, Toughening mechanisms in epoxy-silica nanocomposites (ESNs), *Polymer* **50** (2009), 4895–4905.
[14] J. Baller, N. Becker, M. Ziehmer, M. Thomassey, B. Zielinski, U. Müller and R. Sanctuary, Interactions between silica nanoparticles and an epoxy resin before and during network formation, *Polymer* **50** (2009), 3211–3219.
[15] R.A. Pearson and A.F. Yee, Influence of particle size and particle size distribution on toughening mechanisms in rubber-modified epoxies, *J. Mater. Sci.* **26** (1991), 3828–3844.
[16] R.M. Caddell, *Deformation and Fracture of Solids*, Prentice-Hall, USA, 1980.
[17] A.J. Kinloch and A.C. Taylor, The toughening of cyanate-ester polymers. Part I. Physical modification using particles, fibres and woven-mats, *J. Mater. Sci.* **37** (2002), 433–460.
[18] E.H. Andrews, *Fracture in Polymers*, Oliver and Boyd, Edinburgh, 1968.
[19] B.B. Johnsen, A.J. Kinloch, R.D. Mohammed, A.C. Taylor and S. Sprenger, Toughening mechanisms of nanoparticle-modified epoxy polymers, *Polymer* **48** (2007), 530–541.
[20] D.J. Bray, P. Dittanet, F.J. Guild, A.J. Kinloch, K. Masania, R.A. Pearson and A.C. Taylor, The modelling of the toughening of epoxy polymers via silica nanoparticles: The effects of volume fraction and particle size, *Polymer* **54** (2013), 7022–7032.
[21] Y. Huang and A.J. Kinloch, Modelling of the toughening mechanisms in rubber-modified epoxy polymers: Part I: Finite element analysis and studies, *J. Mater. Sci.* **27** (1992), 2753–2762.
[22] Y. Huang and A.J. Kinloch, Modelling of the toughening mechanisms in rubber-modified epoxy polymers. Part II: A quantitative description of the microstructure–fracture property relationships, *J. Mater. Sci.* **27** (1992), 2763–2769.
[23] A.G. Evans, S. Williams and P.W.R. Beaumont, On the toughness of particulate filled polymers, *J. Mater. Sci.* **20** (1985), 3668–3674.
[24] M.E.J. Dekkers and D. Heikens, Shear band formation in polycarbonate-glass bead composites, *J. Mater. Sci.* **19** (1984), 3271–3275.
[25] M.E.J. Dekkers and D. Heikens, Crazing and shear deformation in glass bead-filled glassy polymers, *J. Mater. Sci.* **20** (1985), 3873–3880.
[26] T.H. Hsieh, A.J. Kinloch, K. Masania, J. Sohn Lee, A.C. Taylor and S. Sprenger, The toughness of epoxy polymers and fibre composites modified with rubber microparticles and silica nanoparticles, *J. Mater. Sci.* **45** (2010), 1193–1210.
[27] T.H. Hsieh, A.J. Kinloch, K. Masania, J. Sohn Lee, A.C. Taylor and S. Sprenger, Erratum to: The toughness of epoxy polymers and fibre composites modified with rubber microparticles and silica nanoparticles, *J. Mater. Sci.* **46** (2011), 4092–4093.
[28] J.N. Sultan and F.J. McGarry, Effect of rubber particle size on deformation mechanisms in glassy epoxy, *Polym. Eng. Sci.* **13** (1973), 29–34.
[29] F.J. Guild and R.J. Young, A predictive model for particulate-filled composite-materials. 1. Hard Particles, *J. Mater. Sci.* **24** (1989), 298–306.
[30] A.J. Kinloch and R.J. Young, *Fracture Behaviour of Polymers*, Elsevier Applied Sciences, London, 1983.
[31] D.A. Norman and R.E. Robertson, Rigid-particle toughening of glassy polymers, *Polymer* **44** (2003), 2351–2362.